INDIAN INSTITUTE OF TECHNOLOGY BOMBAY

DEPARTMENT OF AEROSPACE ENGINEERING

Lagrangian Coherent Structures in Compressible Flows

B.TECH PROJECT

SUBMITTED IN FULFILMENT OF PHASE I II OF B. TECH PROJECT IN THE DEPARTMENT OF AEROSPACE ENGINEERING

Submitted by:
M Vishnu Sankar
18B030013

Supervisor:
Prof. Vineeth Nair

May 2022

Contents

List of Figures

List of Tables

Abstract

Lagrangian Coherent Structures, often abbreviated as LCS, are often referred to as "hidden skeletons of fluid flows which organize the fluid-flow transport"[2]. LCS has been widely studied in incompressible fluid flows, but the understanding of Lagrangian Coherent Structures at unsteady high-speed compressible fluid flows is not yet thoroughly analyzed and studied. This project aims to apply the concept of Finite-Time Lyapunov Exponents (FTLE in short) in unsteady high-speed compressible flows to understand how the coherent structures relate to and interact with the dilatation field of the flow at short and long time intervals. This report includes a brief introduction to Lagrangian Coherent Structures and Finite-Time Lyapunov Exponent field, benchmarking a test case, and the results obtained by applying the framework on compressible doubly-gyre flow and inviscid supersonic flow over an inclined wedge with a stationary oblique shock are discussed at the end, the flow field data for which is obtained by simulation in SU2.

Keywords: Lagrangian Coherent Structures (LCS), Finite-Time Lyapunov Exponents (FTLE), double-gyre, dilatation field, high-speed compressible fluid flows

1 Introduction

Unsteady fluid flows, irrespective of simple or complex, have rich coherent structures present in them, which forms due to the very existence of viscosity in real fluids. Various flow visualisation techniques allow us to identify such coherent structures, but such techniques often may not be always helpful to understand the underlying flow physics. Irrespective of how complicated the flow field may be, there are observable *skeletons* of material surfaces present in fluid flows with dominating viscous effects, such structures are called *Lagrangian Coherent Structures*, the term and idea which was first proposed by *Haller & Yuan*[1]. Finite-Time Lyapunov Exponents is a robust numerical technique method that helps visualise such coherent structures and numerically computes the LCS.

Coherent Structures refers to those flow structures that are not transient in time, alternatively it can be described as those structures that do not dissipate at a short time scale and persist in the flow long enough to influence the flow dynamics[2]. For example, small eddies within boundary layers are not coherent structures as they tend to get dissipated shortly without any significant effect on the flow dynamics. Whereas leading or trailing edge vortices of an oscillating airfoil is a coherent structure as it has a significant influence on the flow dynamics.

The word *Lagrangian* is an indication that the flow structures are tracked both spatially and temporally, unlike the Eulerian framework where only the temporal part is captured in a specific region of interest. According to Haller[1], LCS are "the hidden skeleton of fluid flows" which have a significant influence in mixing and transport of different regions within the fluid. "The LCS approach provides a means of identifying key material lines that organize fluid-flow transport", say Thomas and Haller[2]. "More specifically, the LCS approach is based on the identification of material lines that play the dominant role in attracting and repelling neighboring fluid elements over a selected period of time" as defined by Thomas and Haller[2].

1.1 Understanding Lagrangian Coherent Structures

1.1.1 Material Lines and Manifolds

In 2-D flows, there are lines or curves along which an infinitesimal fluid parcel or fluid material stretches along, or a bunch of fluid parcels tend to repel and separate in different trajectories, or a bunch of fluid parcels tend to attract and cohesively move along very close trajectories. Such lines or curves are termed as *material lines*. In 3-D there are material surfaces. Among the material lines there are two specific sets of lines, one in which the attraction is highest, these lines are *Unstable Manifolds* (may seem quite contrary to the name). And the other set in which the repulsion is highest, these are *Stable Manifolds*. If two fluid parcels which are in vicinity, but on different sides of the stable manifold, begin to advect they separate along the branches of an unstable manifold once they encounter the saddle point. Hence the stable manifold is a repulsive material barrier in forward time. The unstable manifold is an attractive material barrier in forward time, because fluid parcels from the two branches of stable manifold (the one in the top and the one in the bottom of the saddle point) and beginning from the same side attract towards each other along the same branch of the unstable manifold, thus in forward time unstable manifold accumulates fluid parcels along it. In backward time the stable manifold is the attractive material barrier and the unstable manifold is the repulsive material barrier. The

term barrier is intentionally used here as the fluid parcels cannot move cross the manifolds.

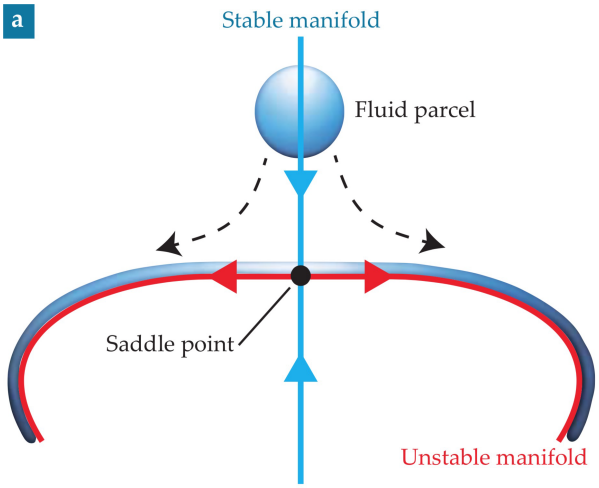

Figure 1: Manifolds, originally published by Thomas & Haller [2]

The notion of stable and unstable manifolds are only well defined for steady and periodic flows. In aperiodic flows, these notions become ill-defined, meaning there are no stable or unstable manifolds as mentioned by Thomas and Haller[2]. The separatrices are analogous to manifolds in time dependant dynamical fluid flow systems. It should be noted here that it is indeed possible to identify fixed points at an instant by freezing the instantaneous velocity field, but that does not help in identifying the separatrices. Hence the emphasis is to find the separatrices by evolving the trajectory of the fluid parcels[4]. For aperiodic flows, the analogous of stable and unstable manifolds are the repulsive and attractive LCS, and these material lines are mutually orthogonal close to the saddle point, just like the manifolds. LCS is also a mobile separatrix (a boundary like structure) with zero mass flux property or with minimum mass leak across it. In a nutshell, "LCS are special surfaces of fluid trajectories that organize the rest of the flow into ordered patterns", as said by Haller in an annual review[1].

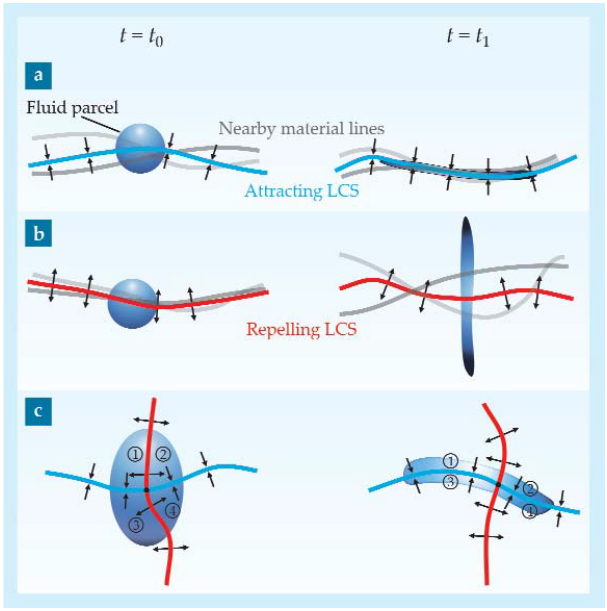

Figure 2: Attracting and Repelling LCS, originally published by Thomas & Haller [2]

1.2 Finite-Time Lyapunov Exponents (FTLE)

The notion of Lyapunov exponents is obtained from the theory of time-dependent dynamical systems. It has a similar notion as the instantaneous rate of separation or attraction between two fluid parcels, except that the FTLE field is not evaluated at an instant but over a finite time that measures the average separation between the trajectories of fluid parcels. To find the FTLE fields the fluid parcels are advected forward or backwards in time. After advecting the particles forward in time, the regions of high separation have higher FTLE constants. When advected backward in time, the fluid parcels that separate are the ones that attract each other in forward time. The regions with the highest FTLE fields are called ridges. In general, the LCS can be equated to FTLE ridges, although some issues might be encountered[2]. More formally, ridges are defined as curves of local maxima in the transverse direction by Shadden(2005)[4].

1.3 Mathematical Framework

1.3.1 Flow Map and Jacobian of Flow Map

The flow field is given by the dynamical system

$$\frac{d\mathbf{x}(t;t_0,\mathbf{x}_0)}{dt} = \mathbf{v}(\mathbf{x},t) \tag{1}$$

Let the initial reference time be t_0 and let $\mathbf{x}(t_0;t_0,\mathbf{x}_0) = \mathbf{x}_0$ be the initial condition. If **v** is independent of time, the system can be analyzed by invariant manifolds of the fixed points. The fixed points of **v** are those $\mathbf{x}^c$ at which $\mathbf{v}(\mathbf{x}^c)$ vanishes[5]. The stable manifolds are trajectories to fixed points whose tangents are eigenvectors of the linearized field of dynamical system only at the vicinity of the fixed points. Stable and Unstable manifolds also act as barriers or ridges that separate distinct regions of motion[5]. In most of real-life fluid flows, there exists no closed-form analytical solution due to the non-linearity present in the governing equation of fluid flows, and **v** in general is time-dependent. Hence as mentioned earlier, the notion of stable and unstable manifold ceases to exist. So the separatrices are identified by allowing the fluid parcels to advect in time, then tracking them and identifying the highest region of separation in forward or backward time. These separatrices are known as Lagrangian Coherent Structures of time-dependent fluid flows, which are direct analogous to the manifolds in time-independent fluid flows[1]. Say at a later time *t*, the position is given as

$$\mathbf{x}(t;t_0,\mathbf{x}_0)) = \mathbf{x}_0 + \int_{t_0}^{t} \mathbf{v}(\mathbf{x},\tau)d\tau \tag{2}$$

In the above equation, the terms at the right side of the equality are represented as $\mathbf{\Phi}_0^t(\mathbf{x}_0)$, known as the flow map. We assume that the velocity data set is smooth. Let $t = T + t_0$ and let's choose *T* such that the perturbations are small. Let the perturbation at the new time instant be $\delta\mathbf{x}(t_0+T)$ and the initial perturbation be $\delta\mathbf{x}(t_0)$, these are related by

$$\delta\mathbf{x}(t_0+T) = \mathbf{\Phi}_0^t(\mathbf{x} + \delta\mathbf{x}(t_0)) - \mathbf{\Phi}_0^t(\mathbf{x}) = \frac{d\mathbf{\Phi}_0^t(\mathbf{x})}{d\mathbf{x}}\delta\mathbf{x}(t_0) + H.O.T \tag{3}$$

where H.O.T refers to higher order terms and the term

$$\frac{d\mathbf{\Phi}_0^t(\mathbf{x})}{d\mathbf{x}}$$

is the deformation gradient, most often referred as jacobian of the flow map, it should be noted here that this jacobian is always invertible as it can never have a zero determinant. The eigenvectors of the jacobian points the direction in which the fluid parcel elongates/compresses the most and the eigenvalues give the magnitude of compression or elongation. If the perturbations are small enough, meaning if they are infinitesimal, the higher order terms are negligible. In that case, the magnitude of the perturbation can be given by,

$$|\delta\mathbf{x}(t_0+T)|^2 = \left\langle \frac{d\mathbf{\Phi}_0^t(\mathbf{x})}{d\mathbf{x}}\delta\mathbf{x}(t_0), \frac{d\mathbf{\Phi}_0^t(\mathbf{x})}{d\mathbf{x}}\delta\mathbf{x}(t_0)\right\rangle = \left\langle \delta\mathbf{x}(t_0), \frac{d\mathbf{\Phi}_0^t(\mathbf{x})}{d\mathbf{x}}^T \frac{d\mathbf{\Phi}_0^t(\mathbf{x})}{d\mathbf{x}}\delta\mathbf{x}(t_0)\right\rangle \quad (4)$$

where T denotes the transpose. We represent

$$\mathbf{C}(\mathbf{x};t_0,T) = \frac{d\mathbf{\Phi}_0^t(\mathbf{x})}{d\mathbf{x}}^T \frac{d\mathbf{\Phi}_0^t(\mathbf{x})}{d\mathbf{x}}$$

for brevity $\mathbf{C}(x;t_0,T)$ is just written as $\mathbf{C}(\mathbf{x})$ and it is known as the *Cauchy-Green strain tensor* which is symmetric. For an incompressible flow $\det(\mathbf{C}) = \lambda_1\,\lambda_2 = 1$. The eigenvectors are ξ_i and the corresponding eigenvalues are $\lambda_i\ (x_0)$, for a two dimensional flow the following relation always holds true.

$$0 < \lambda_1 < 1 < \lambda_2$$

The square root of λ_1 is the magnitude of least compression of the fluid parcel along its principal axis lying in the direction ξ_1 and square root of λ_2 is the magnitude of maximum elongation of the fluid parcel along the principal axis lying along ξ_2 [1]. To compute the jacobian of flow map a central finite difference approximation is used for the points within the boundary and it is done as shown below

$$\frac{d\mathbf{\Phi}_0^t(\mathbf{x})}{d\mathbf{x}} = \begin{bmatrix} \frac{\mathbf{x}^1(t;t_0,\mathbf{x}_0)+\delta_1)-\mathbf{x}^1(t;t_0,\mathbf{x}_0)-\delta_1)}{2|\delta_1|} & \frac{\mathbf{x}^1(t;t_0,\mathbf{x}_0)+\delta_2)-\mathbf{x}^1(t;t_0,\mathbf{x}_0)-\delta_2)}{2|\delta_2|} \\ \frac{\mathbf{x}^2(t;t_0,\mathbf{x}_0)+\delta_1)-\mathbf{x}^2(t;t_0,\mathbf{x}_0)-\delta_1)}{2|\delta_1|} & \frac{\mathbf{x}^2(t;t_0,\mathbf{x}_0)+\delta_2)-\mathbf{x}^2(t;t_0,\mathbf{x}_0)-\delta_2)}{2|\delta_2|} \end{bmatrix} \quad (5)$$

where $\mathbf{x}^1$ and $\mathbf{x}^2$ are the axes of global coordinate system. The local stretching $\sqrt{\lambda_2(\mathbf{x})}$ is observed to grow exponentially with time[1], hence the FTLE field is defined as

$$\boldsymbol{\sigma}_0^t(\mathbf{x}_0) = \frac{1}{T} log\sqrt{max(\lambda_i(x_0))} \quad (6)$$

1.4 Literature Review of FTLE fields on Compressible Flows

One of the early works on studying FTLE fields for compressible flows was studied by Gonzalez and Gaitonde in 2017[6]. It was found that the FTLE field constructed from a small choice of integration time reveals acoustic wave features. They show that the largest bFTLE field ridges capture wave features that are very similar to those in the dilatation field. This result is obtained for a rather simple shock problem in this study which is shown in the subsequent chapters. Another study performed by Han Shuaibin and Shuhai Zhang[7] show that the dilatation field can be re-constructed from the FTLE fields. For small integration time, they establish the following relation

$$\boldsymbol{\sigma}_0^t(\mathbf{x}_0) + \boldsymbol{\gamma}_0^t(\mathbf{x}_0) = \nabla.\mathbf{v} \quad (7)$$

where $\mathbf{v}$ is the velocity field. The summation of the FTLE fields is referred to as *Joint FTLE field*, a term which is also used in this report at the subsequent chapters. It should be noted that this formula is only true for small integration time as higher-order terms are negligible for small time integration.

2 Validating Code with Benchmark Results

In this chapter a standard test case is used to validate the code (developed by *C. P. Premchand, Vineeth Nair*[9]. Modified by the author for this work), then the code is implemented on compressible double-gyre flow field to analyze the relation between dilatation field and FTLE field at small integration time. The double-gyre problem is a standard benchmark problem to test LCS ideas. It is periodic in time and consists of two oppositely rotating vortices (gyres) whose strengths and locations vary periodically. It is worth mentioning here that the velocity field is Eulerian, so changing the frame reference frame to observe or measure the velocity field significantly changes the velocity magnitude and directions. For example, consider an observed fixed to a rotating reference frame. The velocity field of the gyre observed from this velocity field might look like stationery. But the material transport in the gyre is frame independent, so the investigation is to find the frame invariant structures that are responsible for the material transport[2]. Lagrangian coherent structures are responsible for it, which are invariant under coordinate transformations, i.e., translation or rotation[1].

2.1 Double-Gyre Flow

The stream function is given by

$$\psi(x, y, t) = Asin(\pi f(x, t))sin(\pi y)$$

$$f(x, t) = a(t)x^2 + b(t)x$$

$$a(t) = \epsilon sin(\omega t)$$

$$b(t) = 1 - 2\epsilon sin(\omega t)$$

in a domain D = [0,2] x [0,1]. And the velocity field is given by

$$\mathbf{u} = \dot{\mathbf{x}} = -\frac{\partial \psi}{\partial y} = -\pi A sin(\pi f(x, t))cos(\pi y)$$

$$\mathbf{v} = \dot{\mathbf{y}} = \frac{\partial \psi}{\partial x} = \pi A cos(\pi f(x, t))sin(\pi y)\frac{\partial f(x, t)}{\partial x}$$

- A is a factor used to scale the velocity magnitude appropriately
- Non-zero value of ϵ makes the flow time dependent, the gyres expand and contract alternatively in a periodic fashion along the x-direction
- ω is the angular frequency of the two gyres

The value of various parameters are as follows

Parameters	Value
A	0.1
ϵ	0.25
ω	$\frac{2\pi}{10}$

Table 1: Parameters for double-gyre

2.1.1 Computational Framework

Parameter definition	Parameter Symbol	Value
Grid resolution	x_{res}	0.0025 units
Time resolution	t_{res}	0.04 seconds
Integration Time	T	12 seconds

Table 2: Integration Parameter

2.1.2 Plots

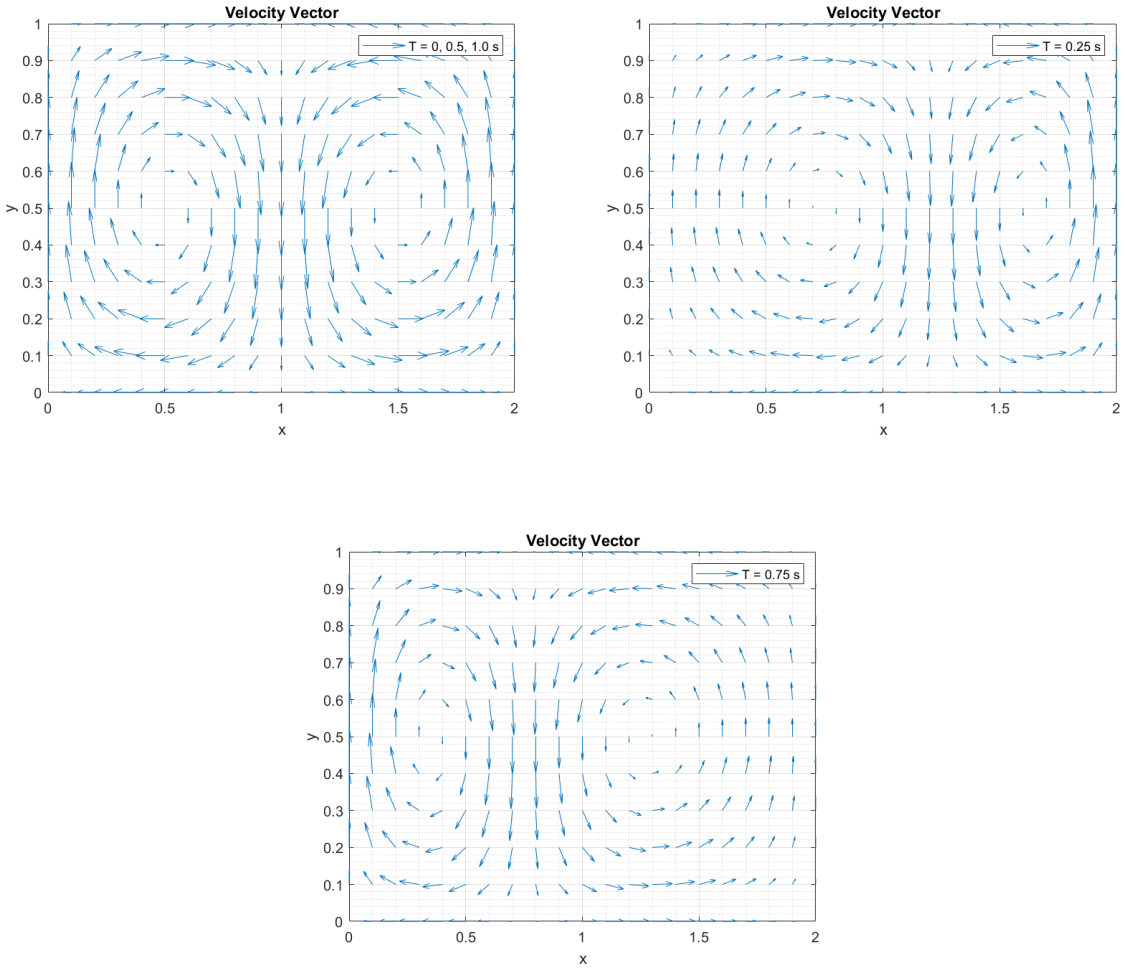

Figure 3: Instantaneous Velocity field in Double-Gyre, Time period = 1 second

As mentioned earlier for $\epsilon \neq 0$ makes the flow time dependent, the gyres expand and contract alternatively in a periodic fashion along the x-direction

2.1.3 Results and Validation

The figures 4 shown below represents the bFTLE ridges, which are the forward time attracting LCS analogous to the unstable manifolds. The image to its right represents the fFTLE ridges, which are the forward time repelling LCS. The particles on one side of the separatrices remain on the same side as the FTLE ridges have minimal mass flux leakage across them.

The figures 5 are those for compressible double-gyre flow. The time step is $1e^{-3}$ seconds, and the rest of the domain remains the same. Although there are a few more equations as shown below to include compressibility

$$\rho = \rho_0 \Big(1 + \zeta \times sin(2pix/\lambda) \times sin(2piy/\lambda) \Big) \tag{8}$$

ζ is the compressibility ratio and λ is the wavelength. In this case $\zeta = 0.2$ and $\lambda = 0.2$. In addition, each component of the velocity is multiplied with ρ_0/ρ to conserve momentum, more about this is given by Vicente Pérez-Muñuzuri[8]

$$\mathbf{u} = -\frac{\partial \psi}{\partial y} = -\pi A sin(\pi f(x,t)) cos(\pi y) \times \frac{\rho_0}{\rho}$$

$$\mathbf{v} = \frac{\partial \psi}{\partial x} = \pi A cos(\pi f(x,t)) sin(\pi y) \frac{\partial f(x,t)}{\partial x} \times \frac{\rho_0}{\rho}$$

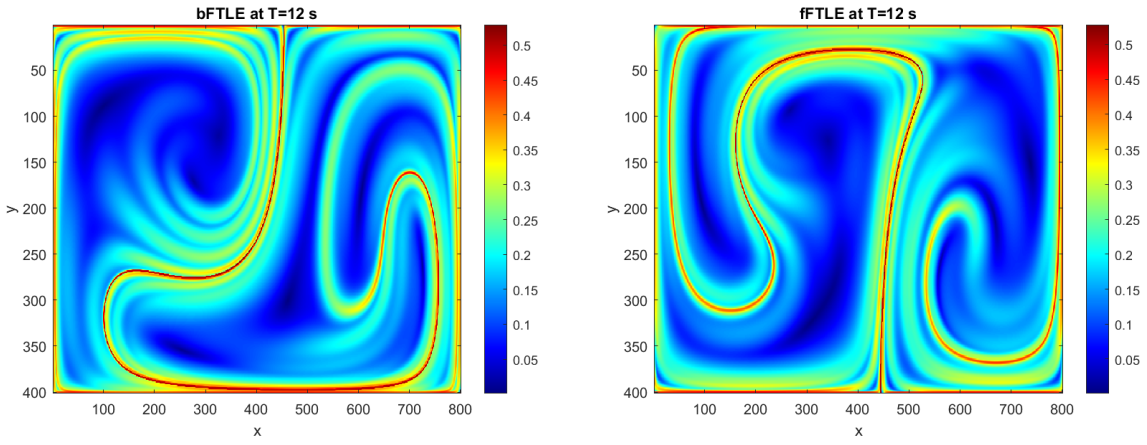

Figure 4: FTLE Incompressible double-gyre

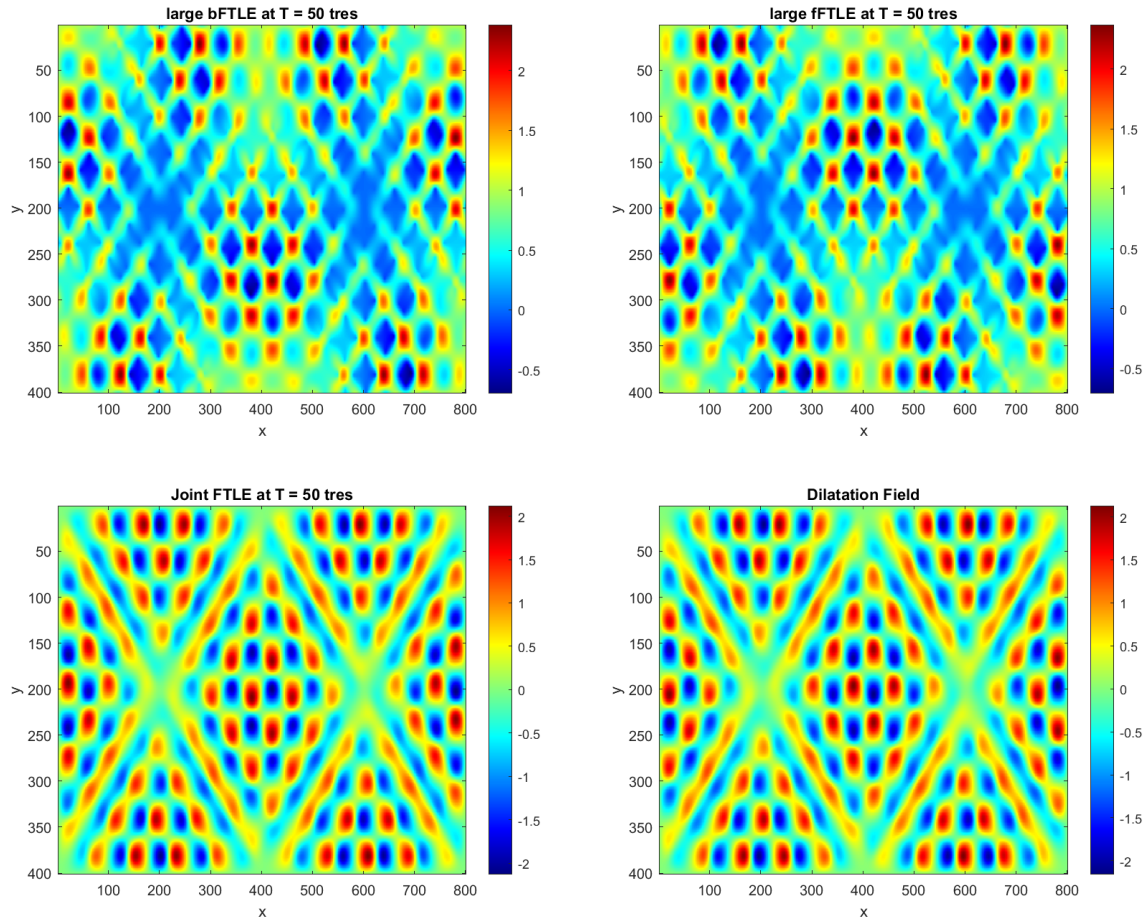

Figure 5: FTLE Compressible double-gyre and Dilatation

Here the joint FTLE field is re-constructed by subtracting the largest backward FTLE field from the largest forward FTLE field. More about this is given in the next chapter.

3 FTLE Analysis on a Oblique Shock

In this chapter the Finite Time Lyapunov Exponent field is calculated for a steady state supersonic oblique shock that is developed over a wedge of 10^0 and results are discussed at the end of this chapter.

3.1 Setup in SU2

In an early study done by the author of this report, a Grid Independent Test was carried out to find the approximate number of cells to run an economical simulation. Mesh even with 1900 number of cells produce reasonably accurate simulation results, so to generate the FTLE plots about 3700 grid points were used to get the velocity data field. This data is shown below for completeness

M_∞	2.0
P_∞	10^5
T_∞	300

Table 3: Free-stream Value

M_2	1.64052
P_2	170658 Pa
T_2	351.045 K
Shock angle	39.3^0
Wedge angle	10.0^0

Table 4: Theoretical Values from Oblique Shock relation

Solver	Euler
Conv_Num_Method_Flow	**HLLC**
CFL	5
Solver	Euler
Time Marching (unsteady problem)	Dual Time Stepping
Time Step	$5e^{-5}$ s

Table 5: Setup

Mesh Cells	M_2	P_2	T_2
90000	1.6431X	17073X	351.09X
30000	1.6431X	17073X	351.09X
15000	1.6431X	17073X	351.09X
7500	1.643XX	1707XX	351.0XX
1900	1.64XXX	1707XX	351.0XX

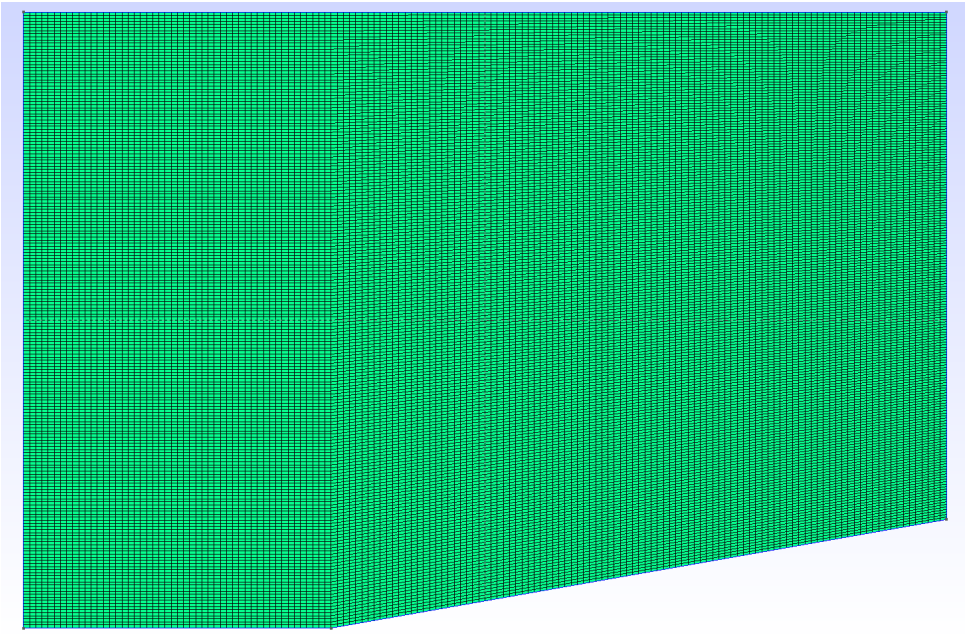

Figure 6: Mesh: 30,000 Cells | Generated in Gmsh

Figure 7: Mach Contour

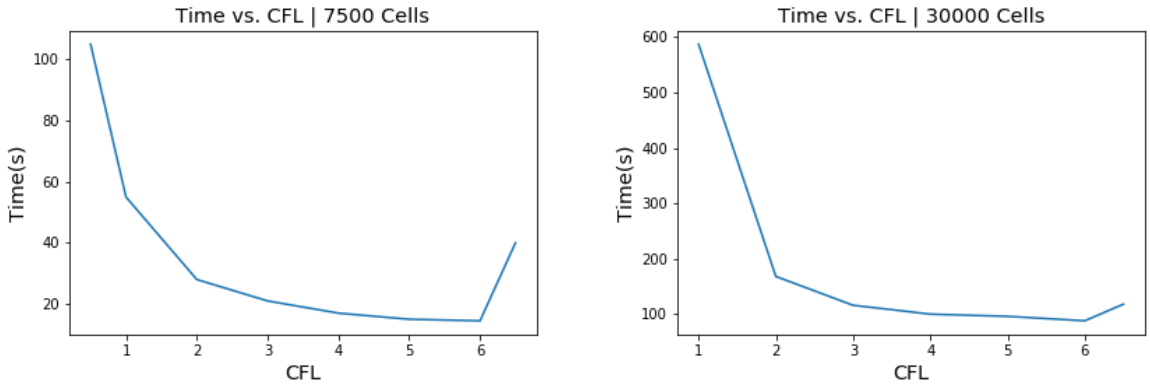

For CFL values lesser than 1, the convergence is very slow and for CFL values greater than 7 the solver diverges. Hence a CFL number of 5 was chosen for the final simulation

t_{res}	$1e^{-5}$ s
x_{res}	0.025
y_{res}	0.02

Table 6: Spatial and Temporal Resolution

The time resolutions were varied between $5e^{-6}s$ to $5e^{-4}s$ and $1e^{-5}s$ was finally chosen to give the best results. However, a window size of at most three could only yield a distinct shock region in the joint FTLE field. For window sizes greater than three, only the biggest backward FTLE contained the shock structure similar to the dilatation field. The spatial resolution could be improved to get more cleaner FTLE fields, a comparison study can be done in the next stage of BTP. To find the jacobian of flow map, the step size was chosen to be $h = 5e^{-3}$. This value is usually one order less than the gird resolution, a little experimentation is helpful in this regard to give the best results.

3.2 Results

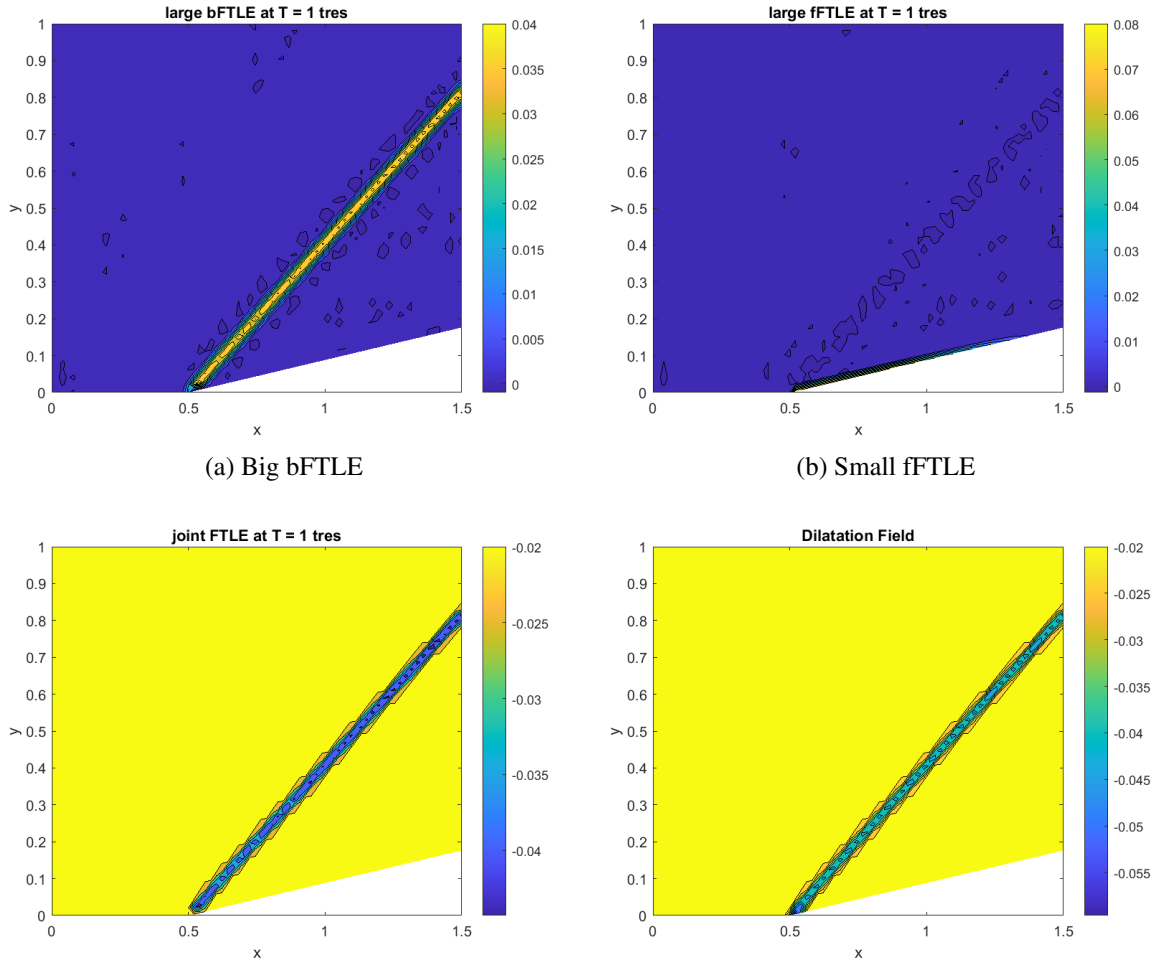

(a) Big bFTLE

(b) Small fFTLE

(c) Joint FTLE

(d) Dilatation

Figure 8: FTLE plots and Dilatation Field, T = 1 tres

NOTE: Here the FTLE fields are multiplied with resolution time because the value of FTLE fields are quite large due to very small resolution time.

The large bFTLE field best captures the shock structure as that in the dilatation field. The reason is backward FTLE is the attractive LCS (recall that is the analogue of unstable manifold) along which fluid parcels converge during forward time. Since a shock wave is region of high compression, it is the region where fluid parcels converge relatively higher than anywhere else in the flow field.
Whereas the forward time FTLE is the repulsive LCS where fluid parcels tend to diverge, hence it does not reveal any shock structure similar to the dilatation field. It is possible that for expansion waves the forward large FTLE can capture the dilatation field more accurately than the backward large FTLE for the same reasons as stated above. For computational purposes the eqn7 is re-written as

$$\boldsymbol{\sigma}_f(\mathbf{x}_0) - \boldsymbol{\sigma}_b(\mathbf{x}_0) = \nabla.\mathbf{v} \tag{9}$$

because the following holds true

$$\boldsymbol{\sigma}_0^{t_0+T}(\mathbf{x}_0) = -\boldsymbol{\gamma}_0^{t_0-T}(\mathbf{x}_0) \tag{10}$$

and

$$\boldsymbol{\gamma}_0^{t_0+T}(\mathbf{x}_0) = -\boldsymbol{\sigma}_0^{t_0-T}(\mathbf{x}_0) \tag{11}$$

where f corresponds to forward FTLE and b corresponds to backward FTLE.

When the joint FTLE is evaluated some type of error seeps in which can be observed in the region where the oblique length of the wedge starts, this can be due to less spatial resolution, so a more spatially re-solved data needs to be obtained and the FLTE ridges need to be computed to check if the error can be avoided.

4 FTLE Analysis on unsteady flows

4.1 Pseudo Code

4.1.1 Pseudo code for calculating forward FTLE structures

Choose appropriate Δt

for $i = 1 : final - time - step$ **do**
$U_x = interpolate(X_{grid}, Y_{grid}, V_x(i\Delta t))$;
$U_y = interpolate(X_{grid}, Y_{grid}, V_y(i\Delta t))$;
$X \leftarrow X + \Delta t \times U_x$
$Y \leftarrow X + \Delta t \times U_y$
Append X and Y to obtain flowmap as Φ_x and Φ_y
end for

Choose appropriate h

$X_{int} = interpolate(X_{grid}, Y_{grid}, \Phi_x)$
$Y_{int} = interpolate(X_{grid}, Y_{grid}, \Phi_y)$;
Calculate $\nabla\Phi$ using central differencing
$CGT = \nabla\Phi^T \times \nabla\Phi$
$\lambda_{max} = max(eig(CGT)$
$\sigma = \frac{1}{T} log\sqrt{max(\lambda_{max})}$

4.1.2 Pseudo code for calculating backward FTLE structures

For calculating the backward FTLE structures only the first half of the code is replaced with:
for $i = final - time - step : 1$ **do**
$U_x = interpolate(X_{grid}, Y_{grid}, V_x(i\Delta t))$;
$U_y = interpolate(X_{grid}, Y_{grid}, V_y(i\Delta t))$;
$X \leftarrow X - \Delta t \times U_x$
$Y \leftarrow X - \Delta t \times U_y$
Append X and Y to obtain flowmap as Φ_x and Φ_y
end for

4.1.3 Evaluating Δt

$$\Delta t = \alpha \times min(\frac{\Delta x, \Delta y}{V_\infty})$$

α is assumed in such a way that the fluid parcels do not move more than half of Δx in a single iteration. Δx is usually chosen outside the boundary layer.

4.1.4 Evaluating h

The value of h is usually taken atleast 10 times smaller than the $min(\delta x, \delta y)$, here we do include the grid points located inside the boundary layer.

4.2 Computational Setup

All the relevant data are generated for NACA 0012 using Ansys Fluent 2021 R2 student version. The following are the details regarding the simulation setup.

$M_{\infty,1}$	0.144
$M_{\infty,2}$	0.5
$R_{\infty,1}$	32,85,000
P_{∞}	10^5
T_{∞}	300
AoA	20^o

Table 7: Free-stream Value

Solver	Unsteady RANS
Turbulence Model	Spalart–Allmaras model
Time Step Size	2.5e^{-4} s
Nodes	120k+
$y+$	between 5-8

Table 8: Setup

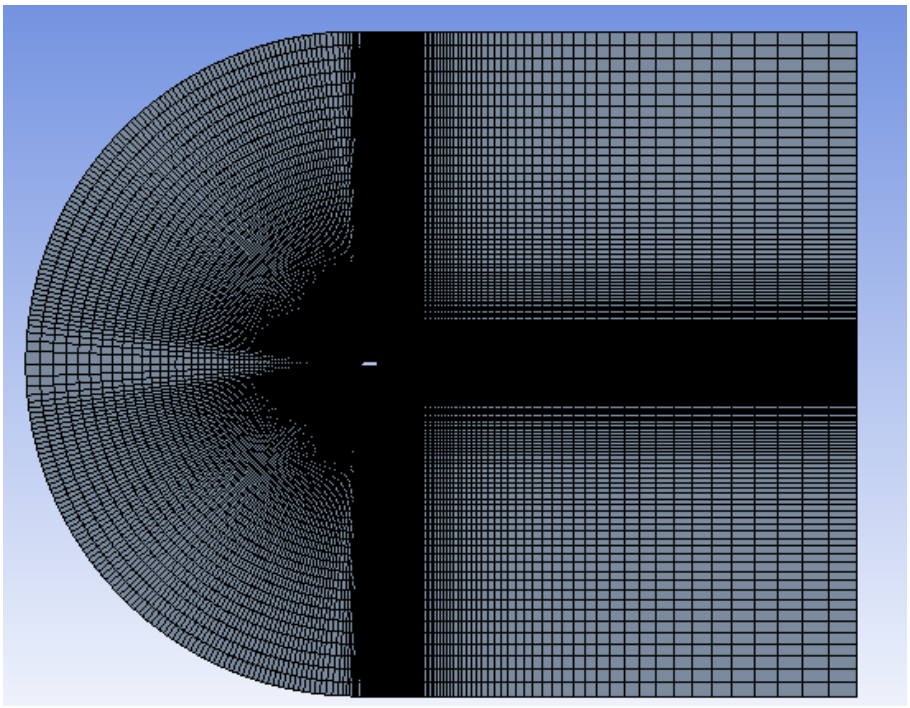

Figure 9: Computational Grid for NACA 0012

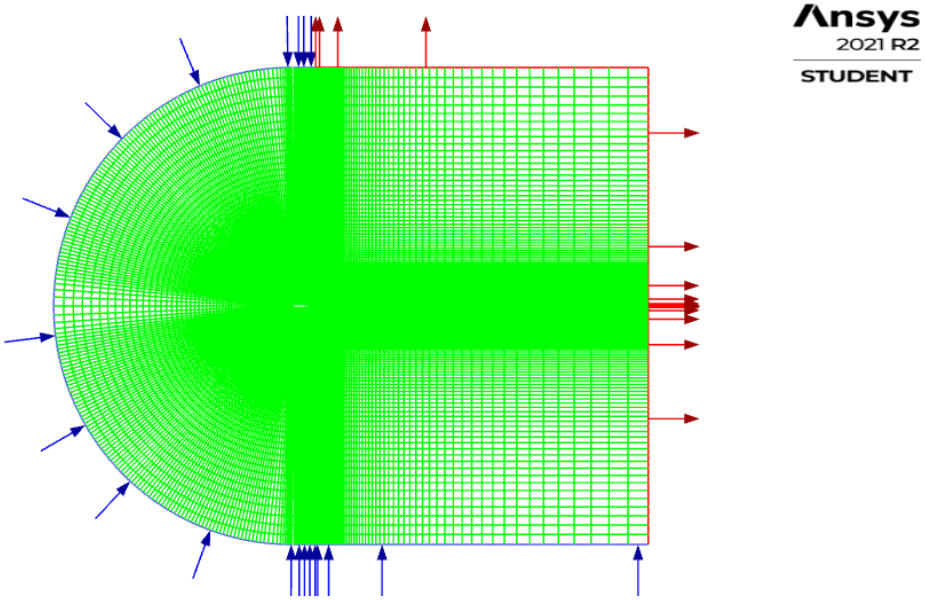

Figure 10: Boundary condition

The SA model works reasonably well with free shear layer flows, hence it is used. The main focus is not on the turbulence modelling aspect so the accuracy of other models is not compared or well tested against the model used here.

5 Results

The solution data is initially in a transient phase where the starting vortex is developed followed by a quick burst of a vortex pair. The solution reaches a steady state with a slight oscillation in the wake structure, thus making the solution slightly unsteady. The FTLE structures are captured for this set of velocity data where the flow is slightly unsteady.

5.1 Case 1: Incompressible flow over NACA 0012, V=50m/s, AoA = 20

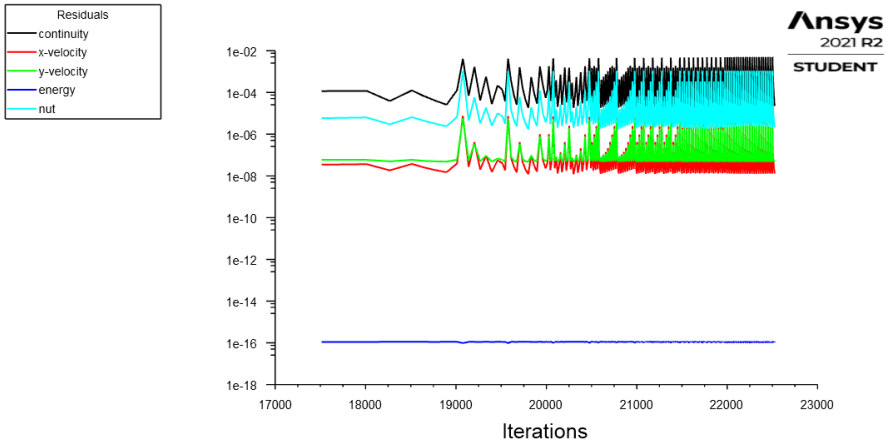

Figure 11: Scaled Residuals Bounded

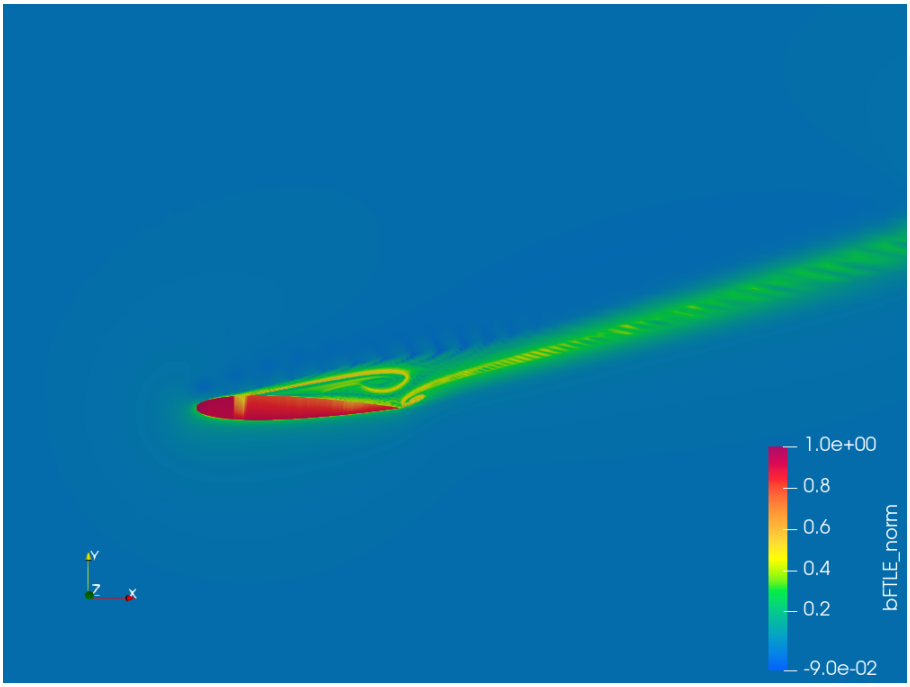

Figure 12: backward FTLE at $30\Delta t$

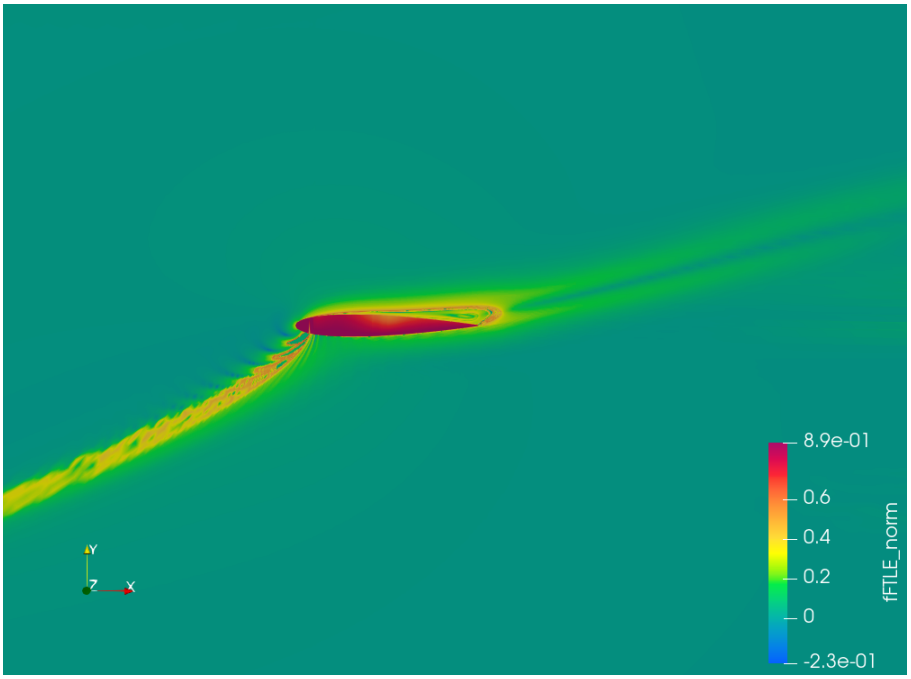

Figure 13: forward FTLE at 30 Δt

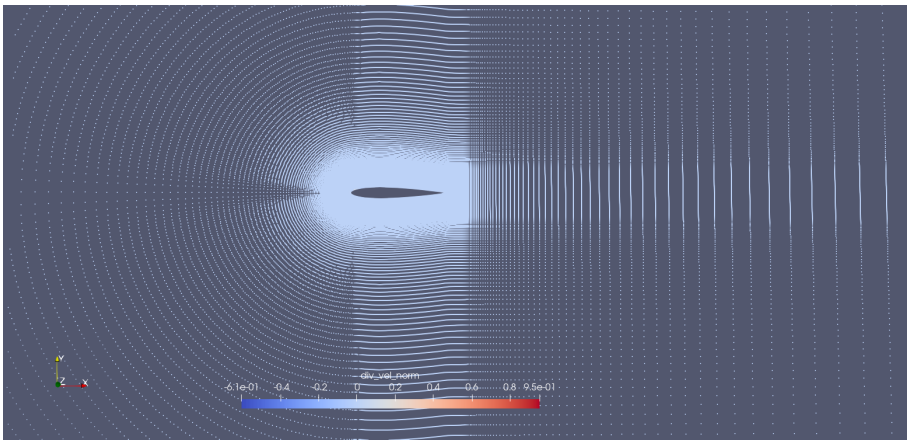

Figure 14: Dilatation Field

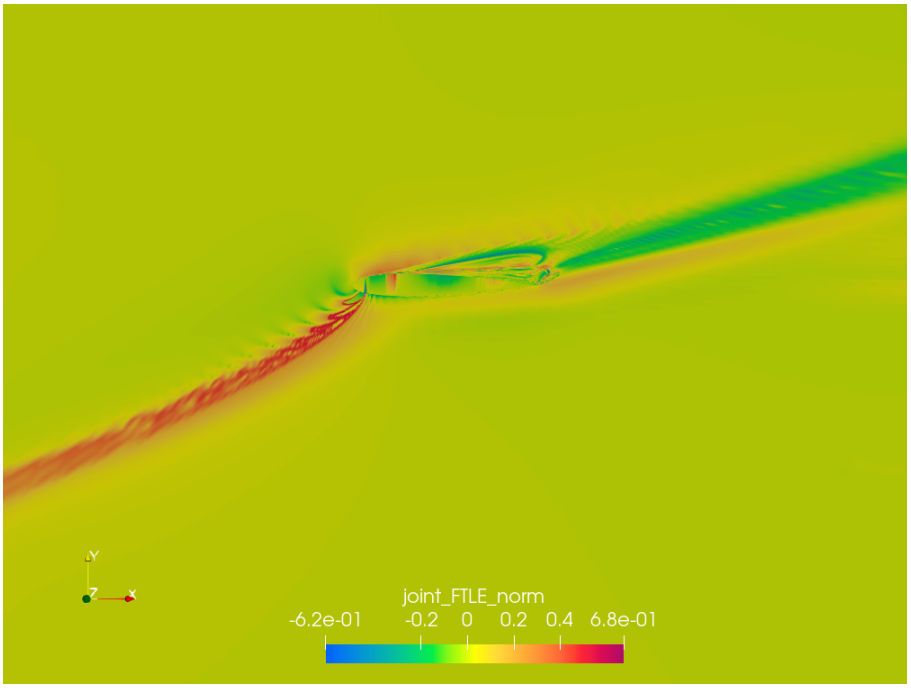

Figure 15: joint FTLE at $30\Delta t$

5.1.1 Observations

Since forward FTLE structures identify the repelling LCSs, referring to figure. 13 of the forward FTLE structure, the repelling LCSs separates the initial fluid domain in two distinct regions due to the flow impinging on the leading edge of the airfoil. The separation bubble is captured by another set of repelling LCSs starting on the top of the airfoil. It should be noted that the repelling LCSs act as *"transport barriers"*.

The attracting LCSs resembles that of a trailing tail in the backward FTLE contour, referring figure:12, it indicates that the flow initially separated into two domains due to the repelling LCSs later move towards the trailing edge and move together alongside of attracting LCSs. Clearly, the dilation field is not the same as the joint FLTE field, which is evident by comparing figure 14 and figure 15

5.2 Case 2: Compressible flow over NACA 0012, V=50m/s, AoA = 20

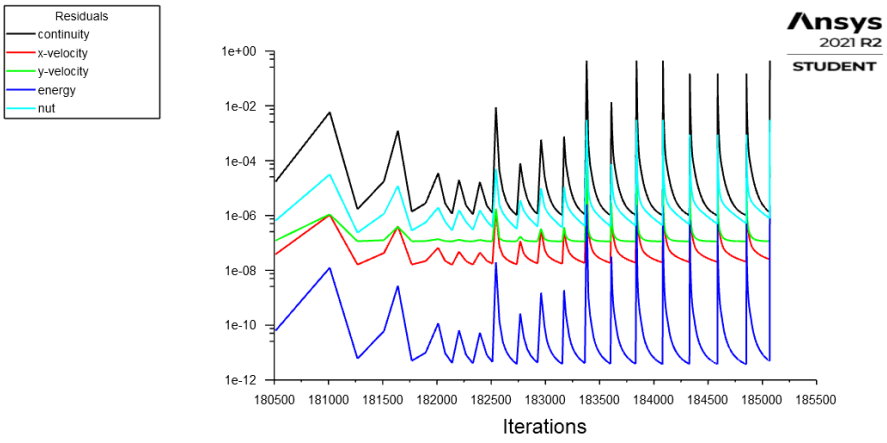

Figure 16: Scaled Residuals Bounded

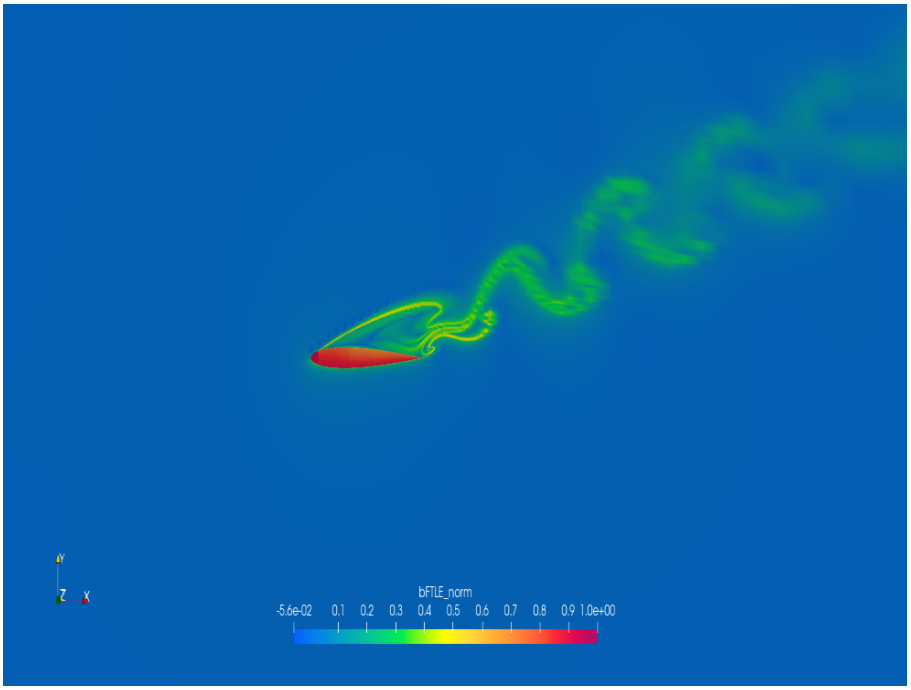

Figure 17: backward FTLE at $50\Delta t$

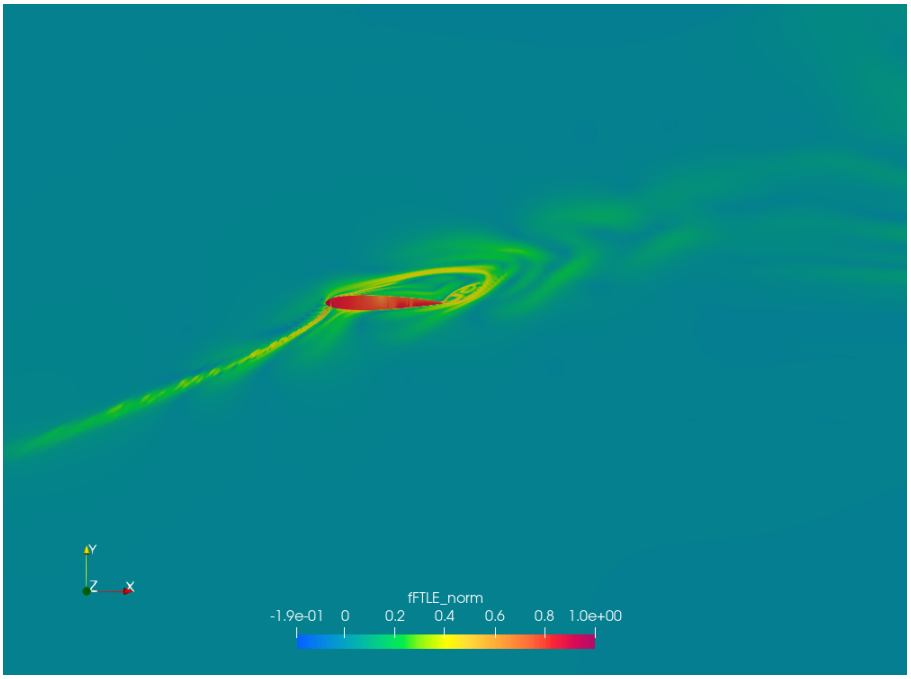

Figure 18: forward FTLE at $50\Delta t$

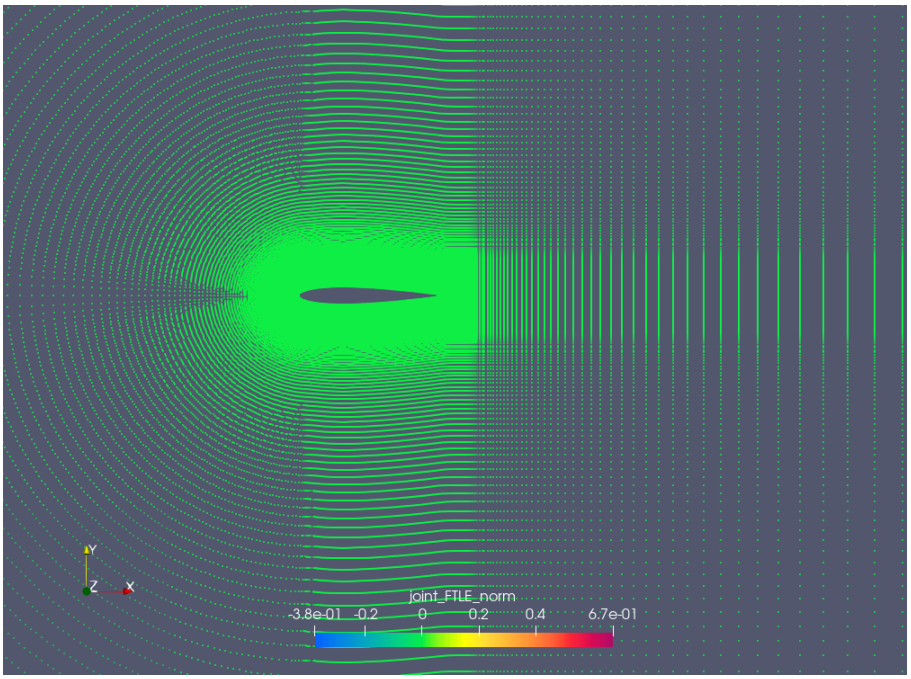

Figure 19: joint FTLE at $1\Delta t$

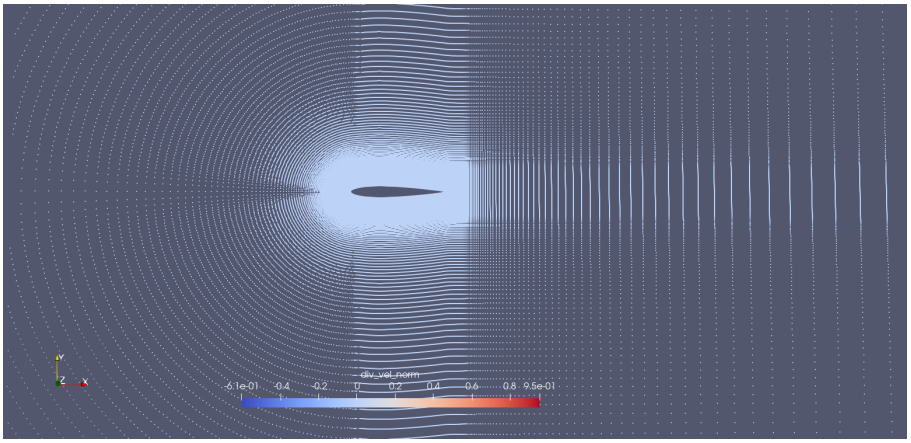

Figure 20: Dilatation Field

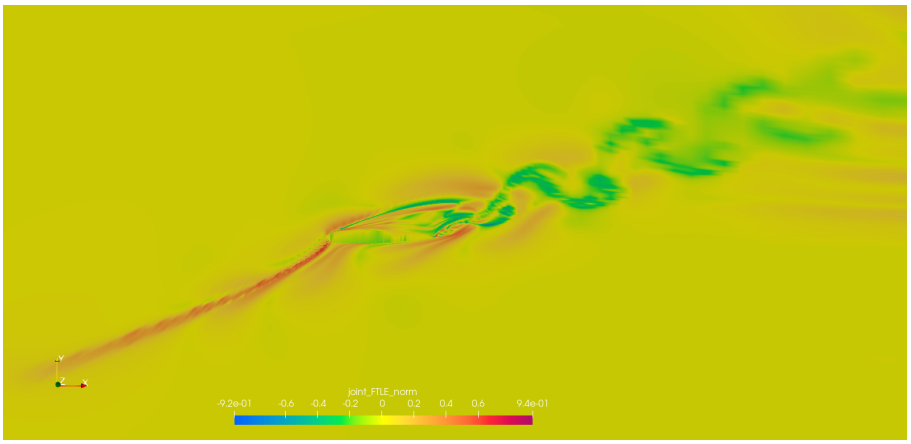

Figure 21: joint FTLE at $50\Delta t$

5.2.1 Observations

The separation bubble in this case is slightly larger than the one of the incompressible case. In figure:17 the attractive LCSs behind the trailing edge is much different from the one in the previous case from figure:12. The attractive LCSs could actually represent small series of vortex being shedded from the trailing edge. The joint FTLE figure: 21 still does not look close to the dilatation field, and does not seems to reveal any new information.

5.3 Conclusion and Future Work

The study done with regards to the oblique shock problem confirms some of the conclusions reached by Gonzalez and Gaitonde[6] and Shuaibin and Shuhai Zhang[7]. The backward FTLE fields capture significant flow features as the dilatation field even at larger window sizes. As the window size increases the area of the shock region is over predicted by the FTLE fields. For this problem window size greater than 3 over-predicts the shock region. We have also reconstructed the dilatation field by obtaining the large FTLE fields by backward and forward integration and the result is in accordance with the formula derived by Shuaibin and Shuhai Zhang[7] for small integration times.

On the other hand the study, presented here in the report, done on the unsteady flow over an airfoil does not concretely support that the dilatation field can be re-constructed from the FTLE fields as per the formulation of Shuaibin and Shuhai Zhang[7]. There can be multiple reasons for this disagreement:

- The acoustic time scale might be smaller than the time resolution used in the computational simulation due to which the FTLE fields may have failed to capture the acoustic effects. In such a case the integration time is longer due to which the relation between the joint FTLE field and the dilatation does not hold anymore as pointed out by Shuaibin and Shuhai Zhang[7]. But the time resolution used in the computational simulation is 0.00025 sec, which seems to be sufficiently smaller to pick up acoustic perturbations.
- The problem we are looking at itself may have very feeble spatial variation of acoustic field associated with it, due to which the FTLE field may be unable to pick up the variation in the acoustic field. The image below is taken for a compressible ideal gas with inlet Mach number at about 0.5. Except only in certain regions very close to the boundary layer, there is almost no sign of spatial variation of the acoustic field.

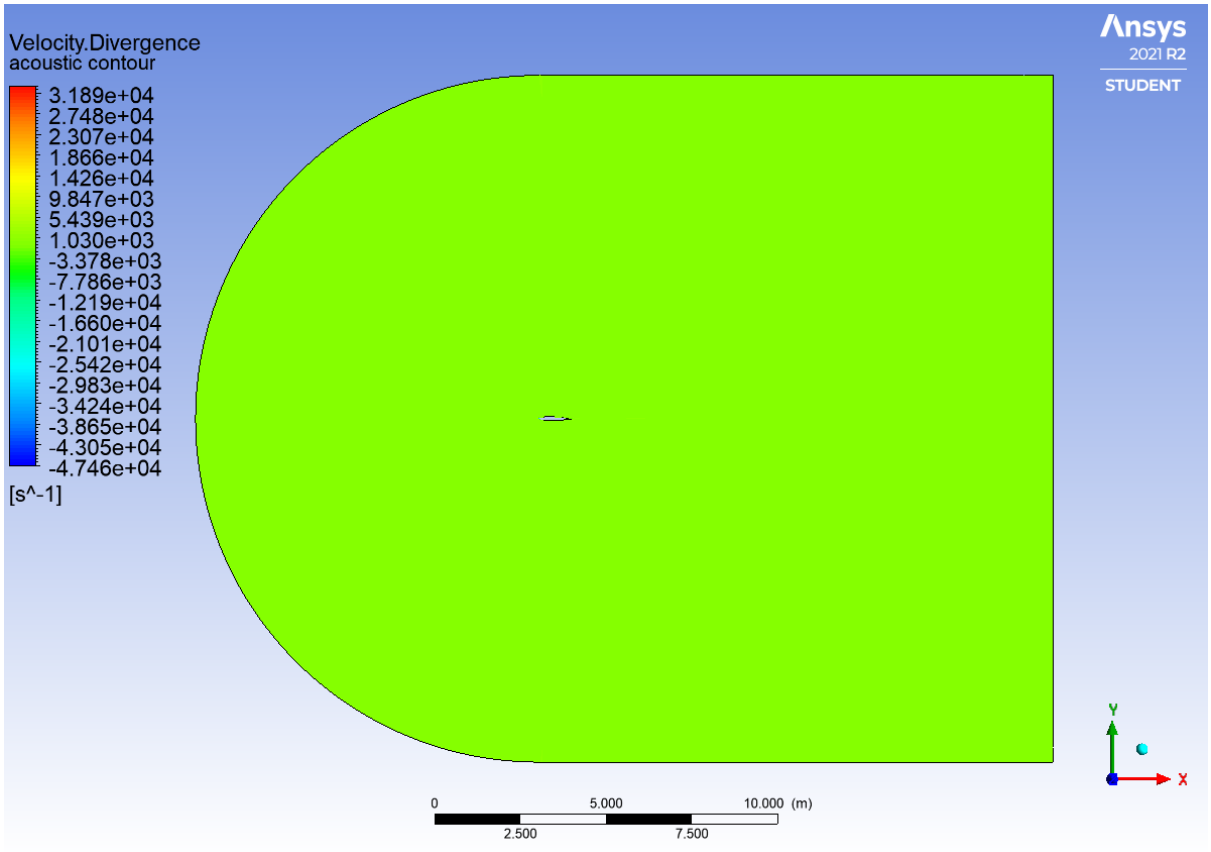

Figure 22: Dilatation field at $50\Delta t$

There is no concrete literature available as to how small the time resolution should be in order to pick up the acoustic perturbation. A possible future work can be to quantitatively estimate the resolution time needed to capture the acoustic perturbations. Another possible research work is derived from the work of Shuaibin and Shuhai Zhang[7], which is to come up with higher order terms to establish a more accurate relation between the acoustic field and the joint FTLE field that holds true for longer integration time.

6 References

[1] George Haller. *"Lagrangian Coherent Structures"*. Annual Review of Fluid Mechanics, January 2015.

[2] Thomas Peacock and George Haller. *"Lagrangian coherent structures: The hidden skeleton of fluid flows"*. Physics Today, February 2013.

[3] Andrew Sven McCall Jr. *Lagrangian Coherent Structures: A Climatological Look*, an undergraduate thesis

[4] S.C. Shadden, F. Lekien, J. E. Marsden, *"Definition and properties of Lagrangian coherent structures from finite-time Lyapunov exponents in two-dimensional aperiodic flows"*. Physica D 212 (2005).

[5] Link to Shadden's website on LCS and FTLE: https://shaddenlab.berkeley.edu/uploads/LCS-tutorial/contents.html

[6] David R González, Datta V Gaitonde. *"Analysis of Compressible Free Shear Layers with Finite-Time Lyapunov Exponents"*. Computers and Fluids, April 2018

[7] Shuaibin Han, Yong Luo, and Shuhai Zhang. *"Relation Between the Finite-Time Lyapunov Exponent and Acoustic Wave"*. AIAA Journal, August 2019

[8] Vicente Pérez-Muñuzuri. *"Mixing and clustering in compressible chaotic stirred flows"*. PHYSICAL REVIEW (2014)

[9] C. P. Premchand, Nitin B. George, Manikandan Raghunathan, Vishnu R. Unni, R. I. Sujith, Vineeth Nair. *"Lagrangian Analysis of Flame Dynamics in the Flow Field of a Bluff Body-Stabilized Combustor"*. Journal of Engineering for Gas Turbines and Power, January 2020.